Buckling Behavior of Conical-Cylindrical Shells and Design Considerations for Launch-Vehicle Applications

Rudd, Michelle Tillotson; Schultz, Marc R.; Bisagni, Chiara

DOI
10.2514/6.2024-0034

Publication date
2024

Document Version
Final published version

Published in
AIAA SciTech Forum and Exposition, 2024

AIAA SciTech Forum
8-12 January 2024, Orlando, FL
AIAA SCITECH 2024 Forum

10.2514/6.2024-0034

Buckling Behavior of Conical-Cylindrical Shells and Design Considerations for Launch-Vehicle Applications

Michelle Tillotson Rudd[1]
NASA Marshall Space Flight Center, Huntsville, AL 35812

Marc R. Schultz[2]
NASA Langley Research Center, Hampton, VA 23681

Chiara Bisagni[3]
Politecnico di Milano, Milan, 20156, Italy

ABSTRACT

Traditionally, launch vehicles are constructed with a series of buckling-prone thin-walled cylindrical and conical shells, in which the buckling behavior of these shells has been well studied and buckling design guidance exists. Conical-cylindrical shell geometry is now being utilized for launch-vehicle stage adapters and payload adapters due to advances in manufacturing and numerical techniques, but there is no available buckling design guidance for this nontraditional combined geometry. In order to provide design recommendations, the buckling behavior and imperfection sensitivity of conical-cylindrical shells and how it differs from the conical and cylindrical components needs to be better understood. From this premise, it is possible to investigate whether or not the buckling knockdown factor guidelines for conical and cylindrical shells outlined in NASA SP-8019 and NASA SP-8007, respectively, are still applicable. The results in this paper will show that the current recommendations are not appropriate in some cases. In addition, it was observed that the large rotations and displacements near the transition between the cone and cylinder can have a larger effect on the buckling load than the presence of radial imperfections for conical-cylindrical shells, which is different than for conical or cylindrical shells. More interesting is the fact that design modifications to increase the buckling capability of a conical-cylindrical shell such as adding reinforcement, which may add mass, will make the shell more sensitive to imperfections. The increased imperfection sensitivity may negate the increase in buckling capability that was thought to be achievable. In the end, it may be more beneficial to design a conical-cylindrical shell in which the buckling behavior is dominated by the more predictable geometric nonlinearity, which may lead to an overall lower buckling load, but a lower knockdown factor may be possible since it will not be as sensitive to the less-known radial imperfections.

I. Introduction

Launch vehicles and payload adapters are mainly comprised of thin-walled cylindrical shells and conical shells. These thin-walled shell structures are constructed with metallic or composite materials, and conical shells are necessary when transitioning from a larger diameter to a small diameter. Mass is a premium on launch vehicles, so it is desirable to save as much mass on primary (core stage, interstage) and secondary structures (payload adapters) by

[1] Aerospace Engineer, Structural Design, Development, and Analysis Branch, AIAA Member.
[2] Supervisory Research Aerospace Engineer, Structural Mechanics, and Concepts Branch, AIAA Associate Fellow.
[3] Professor, Department of Aerospace Science and Technology, Milan, Italy and Guest Professor at Delft University of Technology, Faculty of Aerospace Engineering, Delft, The Netherlands, AIAA Fellow.

maximizing the radius-to-thickness ratio. Therefore, these structures usually have high radius-to-thickness ratios, which make them more susceptible to buckling. State-of-the-art manufacturing and numerical methods also allow designers to consider more nontraditional shapes to save mass and increase volume, for example, combining the conical and cylindrical shells in a single unitized structure. By combining these two sections with a seamless toroidal transition, designers are enabled to remove the heavy, stiff interface ring that often connects the two independent structures, which potentially saves mass. An example of this type of combined structure is the NASA Universal Stage Adapter. Buckling knockdown factor (KDF) recommendations for cylindrical and conical shells are published in NASA SP-8007 and NASA SP-8019, respectively. However, there are no buckling design recommendations for combined conical-cylindrical shells with a toroidal transition.

A reason for the lack of buckling KDFs for conical-cylindrical shells is partially because there is minimal published data that focuses on the buckling behavior of conical-cylindrical shells specifically for the design of aerospace structures. A large majority of the research pertaining to the buckling of conical-cylindrical structures has considered structures under internal and external pressure for the civil and piping industries with applications to civil structures such as silos, pressure vessels, and diffusers. The primary focus of most of these publications is on isotropic conical-cylindrical shells. Internal pressure causes circumferential compressive membrane stresses to develop near the cone-cylinder intersection leading to failures, so authors studied the elastic buckling and plastic collapse loads of isotropic cone-cylinder structures under internal pressure [1-3]. Flores and Godoy performed a numerical study to compare the buckling performance of isotropic cylinders, cones, and cone-cylinder configurations under external pressure [4]. The authors determined that the individual cone and cylinder segments had higher critical buckling pressures than the combined cone-cylinder structures.

Anwen published one of the few available papers regarding the buckling of a conical-cylindrical structures with a toroidal transition segment [5]. The author focused on the effect of the radius of curvature of the toroidal segment on buckling due to external pressure, and its effect on the axial and circumferential stresses at the transition region. Anwen determined that the greater the radius of curvature of the toroidal segment, the greater the critical buckling pressure, and the lower the stress at the joint. Anwen assumed isotropic material properties, considered only external pressure, and axisymmetric imperfections.

Patel, et al. and Singh, et al. [6, 7] studied the buckling and postbuckling characteristics of composite shells in a series of converging and diverging cones and cylinders subjected to torsion, external pressure, axial compression, and thermal loading. The effects of layup, cone angle, and axisymmetric imperfections were interrogated in their research. The effect of the radius of curvature transitioning between the conical and cylindrical sections was not considered. Rudd, et al. recently published a paper on the test and analysis of a composite conical-cylindrical shell under axial compression [8].

There are currently no published NASA recommendations for buckling knockdown factors for conical-cylindrical shells though NASA SP-8007 [9] and NASA SP-8019 [10] do currently provide recommendations for individual cylindrical and conical shells, respectively. The empirical knockdown factors in these documents are used to account for the difference between test and analysis due to the influences of, including but not limited to, radial imperfections and sources of geometric nonlinearity such as large displacements and rotations, and should be applied to the buckling value obtained by a linear eigenvalue analysis. The influence of radial imperfections typically provides a larger contribution to the difference between test and analysis for conical and cylindrical shells than the influence of nonlinear effects on a perfect shell. In general, it is thought that the existing NASA recommendations are often conservative because they do not account for modern materials or manufacturing techniques [11]. It should be noted, however, that the most recent revision of NASA SP-8007 [9] has guidelines for developing design-specific knockdown factors.

The aim of the proposed paper is to explore whether the current buckling design knockdown factor recommendations for launch vehicle structures are applicable to conical-cylindrical shells. First, the individual conical and cylindrical shell components are assessed and compared to the combined conical-cylindrical shell for both isotropic and composite material systems. Next, the recommended buckling knockdown factors in NASA SP-8019 for conical shells and NASA SP-8007 for cylindrical shells are evaluated to understand whether the current knockdown factors are conservative for the combined conical-cylindrical shells. Additionally, sensitivity of conical-cylindrical shells to radial imperfections and geometric nonlinearity under axial compression was assessed. Finally, two experimental buckling tests of composite conical-cylindrical shells are discussed, and the results are used to validate numerical models. The paper concludes with design recommendations and considerations for buckling knockdown factors and provides insight on designing buckling-critical composite conical-cylindrical shells for launch-vehicle applications.

II. Buckling behavior of conical, cylindrical, and conical-cylindrical shells

Traditionally, aerospace structures are comprised of conical and cylindrical shells that are separated by stiff interface rings, which limits much of the interaction between the two structures and allows designers to treat the cone and cylinder components as independent structures. The current knockdown factor recommendations given in NASA SP-8007 and NASA SP-8019 account for difference between test and analysis, which is, in large part, attributable to radial imperfections and geometric nonlinearity. It is of interest to understand if radial imperfections also have a significant effect on the buckling performance of conical-cylindrical shells by determining how radial imperfections and geometric nonlinear effects due to moderate or large rotations and displacements influence the buckling performance. In this section, the linear and nonlinear buckling behavior of conical, cylindrical, and combined conical-cylindrical shells will be compared, and both isotropic and composite material systems will be considered. The study began with numerical analysis of geometrically perfect shells before geometric imperfections were incorporated.

The analyses were completed using the general-purpose finite element software, Abaqus [12]. A mesh convergence study was used to determine that a mesh element size of approximately 5 mm with the four-noded reduced-integration shell element (S4R) was sufficient to capture the buckling behavior for all geometries presented. The Lanczos solver was utilized for the linear eigenvalue analyses and an implicit dynamic nonlinear solver was used to capture the prebuckling and buckling behavior in the nonlinear analyses. The top and bottom edges of the shells had all degrees of freedom fixed, except for the translational degree of freedom at the top edge which allowed for axial displacement.

An aluminum alloy cone with a semi-vertex angle of 15 degrees, a centerline radius of 400 mm, a height of 600 mm, and a wall thickness of 1.43 mm was considered, Figure 1a. The linear eigenvalue for the geometry with an elastic modulus of 71.0 GPa and a Poisson's ratio of 0.33 was 542.4 kN, and the associated eigenmode shape is presented in Figure 1b. Linear eigenvalue analyses are relatively computationally inexpensive, but a computationally intensive geometrically nonlinear analysis can provide a better understanding of the buckling behavior of thin-walled shell structures. The predicted nonlinear buckling load of the isotropic cone geometry was 497.8 kN. That is, the influence of the geometrically nonlinear response reduced the buckling load by 8% as compared to the linear eigenvalue. The predicted deformation shortly after buckling from the nonlinear analysis is shown in Figure 1c. The dark blue dimples at the small diameter end of the cone indicate where the buckling initiated.

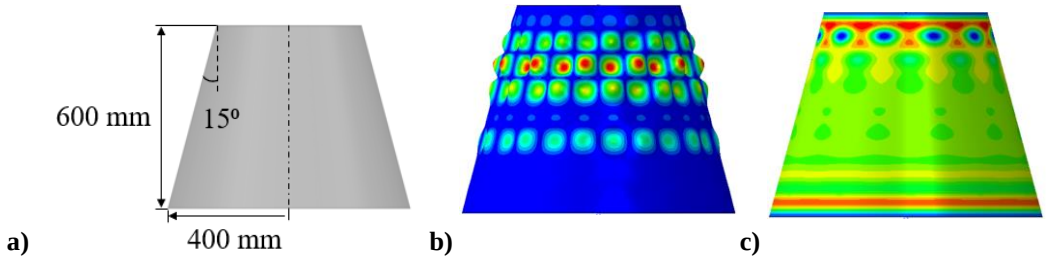

Figure 1. Conical shell: a) geometry; b) first eigenmode; c) radial deformation immediately after buckling.

The analysis procedure described above was repeated for a cylindrical shell with the same height of 600 mm and the same radius of 400 mm and material, Figure 2a. The first linear eigenvalue was predicted to be 581.5 kN, and the first eigenmode is presented in Figure 2b. The geometrically nonlinear buckling load was predicted to be 536.8 kN. The inclusion of large rotations and displacements reduced the buckling load by approximately 8%, which is similar to the conical shell. Figure 2c presents the radial deformations just after buckling from the nonlinear analysis and shows that buckling may occur at ends of the cylinder.

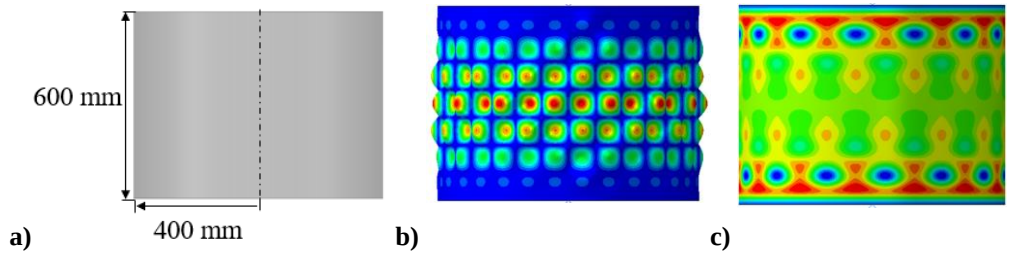

Figure 2. Cylindrical shell: a) geometry; b) first eigenmode; c) radial deformation immediately after buckling.

To create the conical-cylindrical shell for this study, the cone and cylinder geometries presented above were stacked on top of one another and combined, Figure 3a. The linear eigenvalue for this conical-cylindrical shell was 516.8 kN and the associated linear eigenmode is presented in Figure 3b. The geometrically nonlinear buckling load was 261.5 kN, which is approximately 50% of the linear eigenvalue load. This reduction is much greater than the 8% observed for the individual cone and cylinder components. The radial deformations immediately after buckling for the conical-cylindrical shell in Figure 3c shows that buckling initiated near the junction between the cone and cylinder.

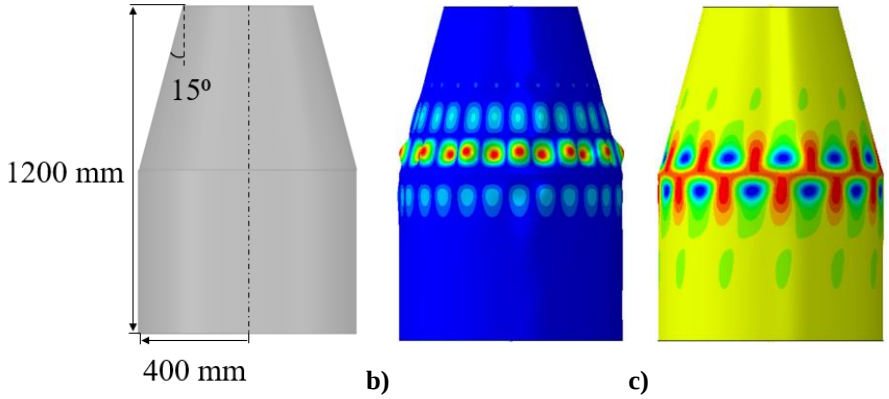

Figure 3. Isotropic conical-cylindrical shell: a) geometry; b) first eigenmode; c) radial deformation immediately after buckling.

Since it is well known that the difference between test and analysis for conical and cylindrical shells can be largely attributed to the presence of radial imperfections, analyses were performed to understand whether conical-cylindrical shells share a similar sensitivity to radial imperfections. Using the geometry presented in Fig. 3a, an imperfection shape of the first eigenmode for the conical, cylindrical, and conical-cylindrical shell was used as the radial imperfection. The first eigenmode shape was selected as the imperfection shape because the first eigenmode or weighted combinations of eigenmodes are commonly used in practice to assess the imperfection sensitivity of an aerospace shell structure. The eigenmode shapes are presented in Figure 1b, Figure 2b, and Figure 3b for the conical, cylindrical, and conical-cylindrical shells, respectively. The amplitude of the imperfection was chosen to be to 10% of the 1.43 mm thickness.

The KDFs given in NASA SP-8007 and NASA SP-8019 are correlation factors ranging between zero and one that relate the idealized analytical eigenvalue buckling loads to the recommended buckling design loads. The KDFs recommend are the lower-bound recommendation based on a series of experimental tests that were normalized by the linear eigenvalue. The normalized buckling load, which herein is defined as the numerically predicted geometrically nonlinear buckling load with imperfections divided by the numerically predicted linear eigenvalue, is used as a way to relate the results of the present study with the KDFs in NASA SP-8007 and NASA SP-8019. The normalized buckling load can be directly compared with the KDF even though they were obtained in different ways.

The load versus displacement curves for the conical, cylindrical, and conical-cylindrical shells with imperfections are presented in Figure 4 along with the linear eigenvalue and nonlinear curves for the three shells without imperfections. The normalized buckling load for the imperfect cone, the buckling load from the nonlinear analysis with imperfections, 288.0 kN, divided by the linear eigenvalue, 542.4 kN, is equal to 0.53. The normalized buckling load for the cylinder with imperfections was 310.0 kN divided by the linear eigenvalue 581.5 kN, which equals 0.53. The conical shell and cylindrical shell have the same normalized buckling loads. However, the nonlinear buckling load with imperfections for the conical-cylindrical shell was 221.6 kN, which results in a normalized buckling load of 0.43.

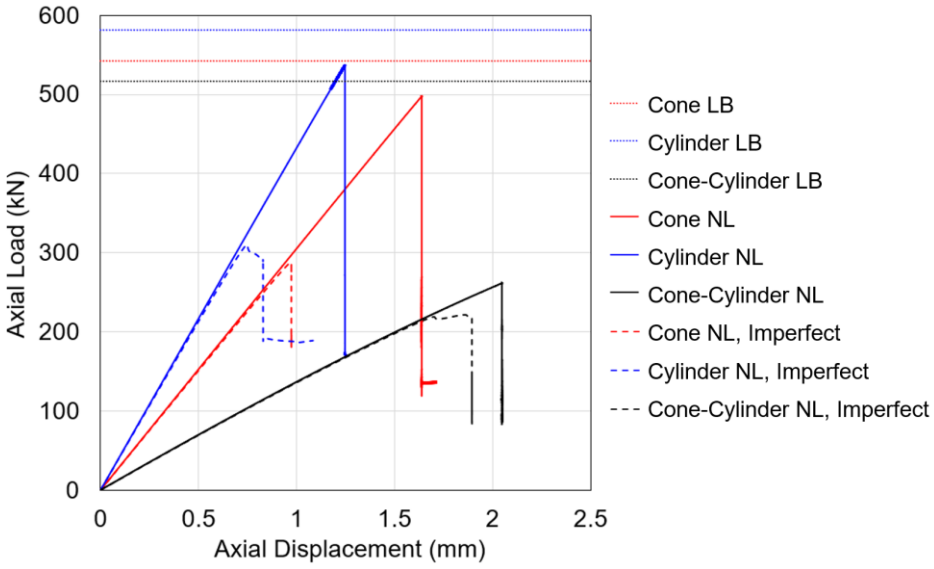

Figure 4. Linear eigenvalue (LB) curves, nonlinear buckling (NL) curves, and imperfection nonlinear buckling curves for the isotropic conical, cylindrical, and conical-cylindrical shells.

The results of these nonlinear analyses of imperfect shells confirm that the presence of radial imperfections can significantly reduce the buckling capability for the conical and cylindrical shells. The inclusion of the eigenmode imperfection decreased the predicted buckling load by 42%, which is significant compared the 8% reduction in load due to the inclusion geometric nonlinearities for the cone and cylinder. These results contrast with the results from the conical-cylindrical shell where the inclusion of radial imperfections reduced the buckling by only 15% and the inclusion of nonlinear geometry reduced the buckling load by 49%. These results indicate that conical-cylindrical shells may be not as sensitive to geometric imperfections as conical and cylindrical shell components.

From a launch vehicle design perspective, the NASA-recommended KDFs for the studied conical and cylindrical shells are 0.33 and 0.42, respectively. The normalized buckling loads for the conical and cylindrical shells were both 0.53. Comparing the normalized buckling loads of 0.53 to the recommended KDFs, NASA SP-8007 and 8019 could be considered conservative. On the other hand, the normalized buckling load for the conical-cylindrical shell of 0.43, may not be considered conservative when compared to the KDF recommended for the cylindrical shell. The conical shell KDF is still conservative.

To assess if the large difference between the linear and nonlinear analyses is specific to the combined conical-cylindrical shell geometry, similar analyses were repeated with a shell of the same dimensions with Hexcel's IM7/8552-1 carbon-epoxy material system [13]. A composite quasi-isotropic layup of $[45/\text{-}45/90/0]_S$ with the unidirectional carbon fiber tape material system was assumed in the analyses. In order to maintain the same radius-to-thickness ratio as the isotropic structure, the total laminate thickness was 1.43 mm, so each ply had a 0.173-mm thickness. A modulus of elasticity of 140.9 MPa in the fiber direction, a modulus of elasticity transverse to the fiber direction of 9.72 MPa, a shear modulus equal to 4.69 MPa, and an in-plane Poisson's ratio of 0.356 were used in the analyses.

A linear eigenvalue analysis and a geometrically nonlinear analysis were completed, followed by a geometrically nonlinear analysis with imperfections. The linear eigenvalue for this structure was 330.8 kN and the associated eigenmode is shown in Figure 5a. The nonlinear buckling load for this configuration was 186.0 kN and the radial deformation shape at this load is in Figure 5b. As with the isotropic case, the first eigenmode was used as an imperfection and applied to the geometry with an amplitude 10% of the total laminate thickness. The predicted nonlinear buckling load with the imperfect geometry was also 186.0 kN, which results in a normalized buckling load of 0.56. The radial displacement shape at buckling is presented in Figure 5c. The addition of radial imperfections essentially had no effect on the buckling load for the composite conical-cylindrical shell, and it did not significantly influence the location of buckling initiation. The dark blue dimples, which represent inward dimples and buckling locations, are still around the conical-cylindrical junction in both Figure 5b and Figure 5c. In a manner similar to the isotropic analyses, the inclusion of nonlinear geometric effects had a greater influence on the buckling load than the inclusion of imperfections for this geometry. From comparison of the buckling predictions for the isotropic and composite conical-cylindrical shells, it would appear that the buckling behavior of conical-cylindrical shells is

influenced more by the chosen geometry than the material system. Additionally, using the first eigenmode shape as the imperfection shape to determine the imperfection sensitivity may not be considered the most conservative approach since it did not affect the buckling load for the composite conical-cylindrical shell.

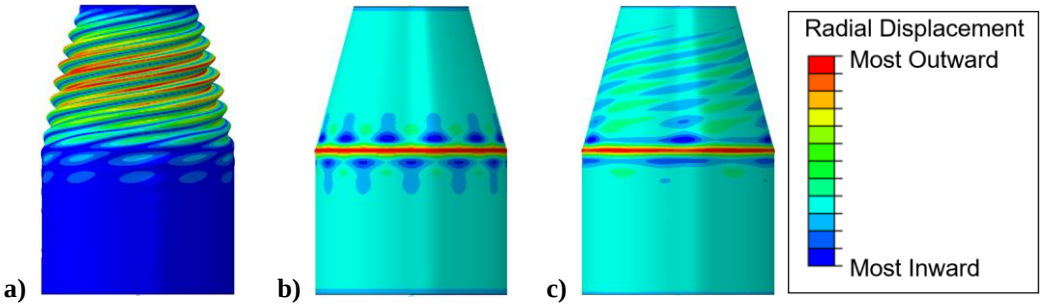

Figure 5. Composite conical-cylindrical shell radial displacement shapes: a) first eigenmode; b) at buckling without imperfections; c) at buckling with imperfections.

III. Effect of the transition region on the buckling behavior of composite conical-cylindrical shell

Since buckling initiates near the transition region for the configurations with and without imperfections for both isotropic and composite material systems, it would appear this region is important to the buckling response of conical-cylindrical shells. To investigate the importance of this region further, the radius of curvature between the conical and cylindrical shells was increased to create a more gradual transition between the components by creating a toroidal transition region as shown in Figure 6. The radius of curvature, ρ, for the geometry previously investigated was equal to 0 mm, Figure 6a. Radii of curvatures of 200 mm, 400 mm, and 800 mm were also investigated, Figure 6b - Figure 6d. The radius of the cylinder was 400 mm, and the height was 1200 mm to be consistent with the previously considered geometry. Composite material properties were considered for the following buckling analyses.

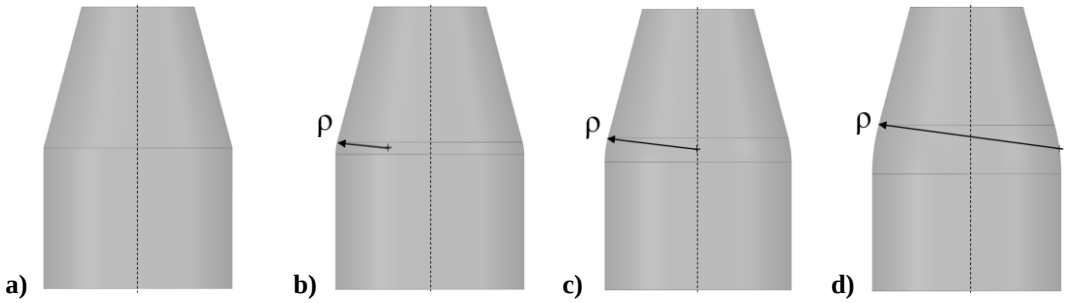

Figure 6. Geometry with different radii of curvatures: a) ρ = 0 mm; b) ρ = 200 mm; c) ρ = 400 mm; d) ρ = 800 mm.

The results for the linear and nonlinear analyses for the composite conical-cylindrical shells for each radius of curvature is presented in Table 1 and Figure 7. It can be observed in the table that as the transition between the cone and cylinder becomes more rounded, i.e., the radius of curvature increases, the linear eigenvalues were essentially unchanged and the nonlinear buckling loads increased. It is postulated that, as the radius of curvature increases, there is a reduction in the large rotations and displacements that occur near the transition region, which makes the nonlinear buckling load in better agreement with the linear eigenvalue. A result of the large rotations near the transition region is a decreasing in stiffness with decreasing transition-region radius, which can be seen in Figure 7 as a decreasing slope of the nonlinear load-displacement curves with decreasing transition-region radius. In the following discussion, the configuration with the radius of curvature equal to 400 mm will be the baseline for comparison.

Table 1. The linear and nonlinear buckling loads and normalized buckling load of a composite conical-cylindrical shell with different radii of curvatures.

Radius of curvature of transition region, ρ (mm)	Linear eigenvalue (kN)	Nonlinear (kN)
0	330.8	186.0
200	330.9	229.9
400	331.0	271.7
800	331.0	300.8

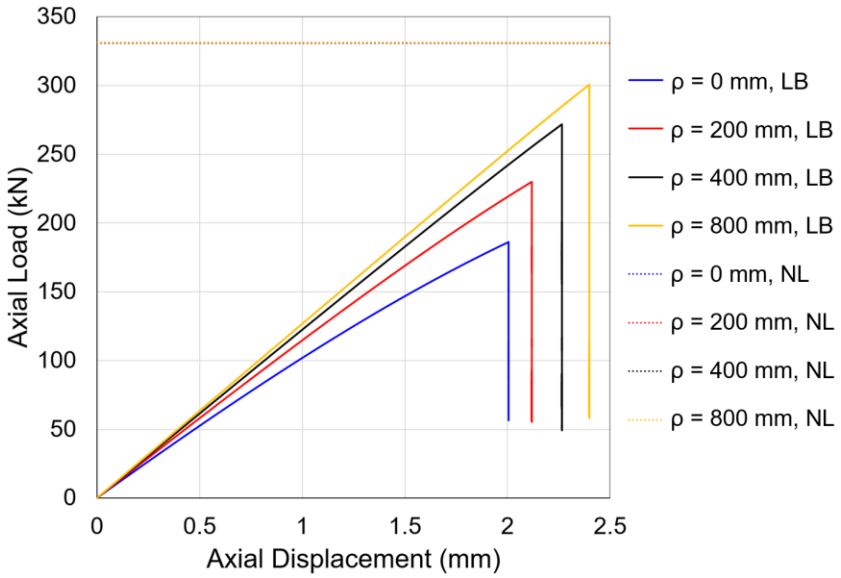

Figure 7. Linear eigenvalue (LB) curves and nonlinear buckling (NL) curves for composite conical-cylindrical shells with different radius of curvatures.

After the effect of the transition region on the buckling behavior was studied, an investigation of the imperfection sensitivity was completed. The composite conical-cylindrical shell with a radius of curvature of 400 mm was investigated and will be referred to as the baseline. The imperfection shape used was the first eigenmode, shown as Figure 8, since it is a common shape used to assess sensitivity to radial imperfections. Imperfection amplitudes equal to 10% and 20% of the wall thickness were considered. The values for the nonlinear buckling loads and normalized buckling loads are presented in Table 2. The load verses displacement curves are presented in Figure 9.

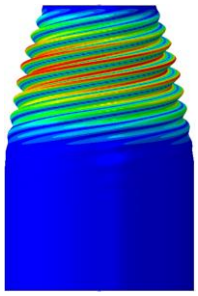

Figure 8. First linear eigenmode of a composite conical-cylindrical shell with ρ = 400 mm.

Table 2. The linear and nonlinear buckling loads and normalized buckling load of a composite conical-cylindrical shell with different imperfection amplitudes.

Imperfection	Linear eigenvalue (kN)	Nonlinear (kN)	Normalized
Baseline	331.0	271.7	0.82
Eigenmode 10%		213.4	0.65
Eigenmode 20%		160.5	0.48

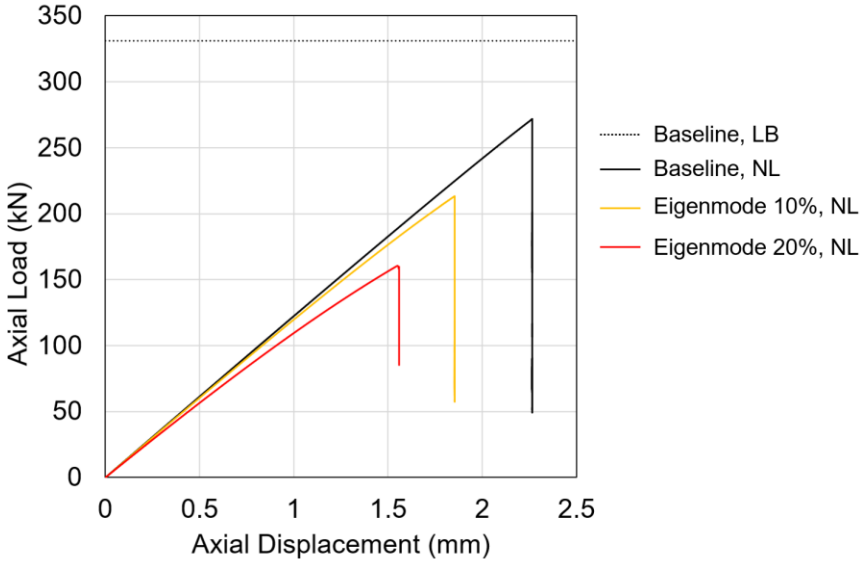

Figure 9. Linear eigenvalue (LB) curve and nonlinear buckling (NL) curves for the composite conical-cylindrical shell with ρ = 400 mm without imperfections and with imperfections.

From Table 2 and Figure 9 it can be observed that the composite conical-cylindrical shell with a radius of curvature of 400 mm, baseline configuration, was more imperfection sensitive than with a radius of curvature of 0 mm. The nonlinear buckling load for the baseline configuration without imperfections was 271.7 kN. The nonlinear buckling load with an imperfection amplitude of 10% was 213.4 kN. It was previously shown that, for no radius of curvature between the cone and cylinder components (ρ = 0 mm), the buckling load with imperfections was 186.0 kN and there was no reduction in load carrying capability when a same imperfection amplitude was included in the analysis. This suggests that, as the transition-region radius of curvature increases, the perfect-geometry buckling load increases, and so does the imperfection sensitivity. In addition, it should be noted that the normalized buckling load for the analyses with a 20% imperfection amplitude was 0.48. The orthotropic-cylinder KDF calculated using NASA-SP-8007 is 0.43, which may not be considered conservative.

With composite material systems, it is possible to reinforce localized areas of a structure with additional plies. For example, it may be advantageous to increase the stiffness of the transition region, and this could affect the buckling behavior and imperfection sensitivity of the composite conical-cylindrical shell. To investigate the influence of localized reinforcement of the transition region further, four reinforcement cases were considered ranging in relative stiffness of less stiff to more stiff, as shown in Table 3. The area where reinforcement was applied is highlighted in red in Figure 10. The baseline configuration has a radius of curvature equal to 400 mm and no additional plies. The increase in mass from the baseline composite-conical cylindrical shell due to the additional plies is also shown.

Table 3. Transition reinforcement layups and associated percent increase in mass.

Reinforcement	Layup	% Increase in mass
Baseline	$[45/-45/90/0]_S$	-
Reinforcement 1	[**90**/45/-45/90/0/0/90/-45/45]	1.1%
Reinforcement 2	$[\mathbf{90}/45/-45/90/0]_S$	2.2%
Reinforcement 3	$[\mathbf{90/0}/45/-45/90/0]_S$	4.7%
Reinforcement 4	$[\mathbf{90/0/0/90}/45/-45/90/0]_S$	9.4%

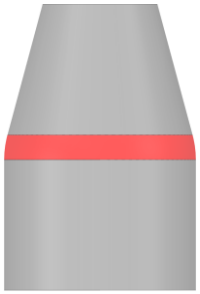

Figure 10. Region where reinforcement was applied highlighted in red.

The results from the linear eigenvalue analyses and nonlinear buckling analyses for the composite conical cylindrical shells with and without reinforcement are presented in
Table 4 and Figure 10. The linear eigenvalue for all levels of reinforcement were the same, similar to what was observed when the radius of curvature was increased. The nonlinear buckling load, on the other hand, increases as additional plies are added, but only up to the linear eigenvalue. In this case, after Reinforcement 3 the nonlinear buckling load seems to converge to the linear eigenvalue as seen in Figure 11. The overall shell stiffness was increased with Reinforcement 4, but the buckling load was not significantly increased. Therefore, there seems to be a point of diminishing returns when comparing the mass of the additional reinforcement to the increase in buckling load.

Table 4. Linear eigenvalue and nonlinear buckling load for composite conical-cylindrical shell with different transition-region reinforcement layups.

Reinforcement	Linear eigenvalue (kN)	Nonlinear (kN)
Baseline	331.0	271.7
Reinforcement 1	331.0	296.9
Reinforcement 2	331.0	319.8
Reinforcement 3	331.0	331.9
Reinforcement 4	331.0	332.2

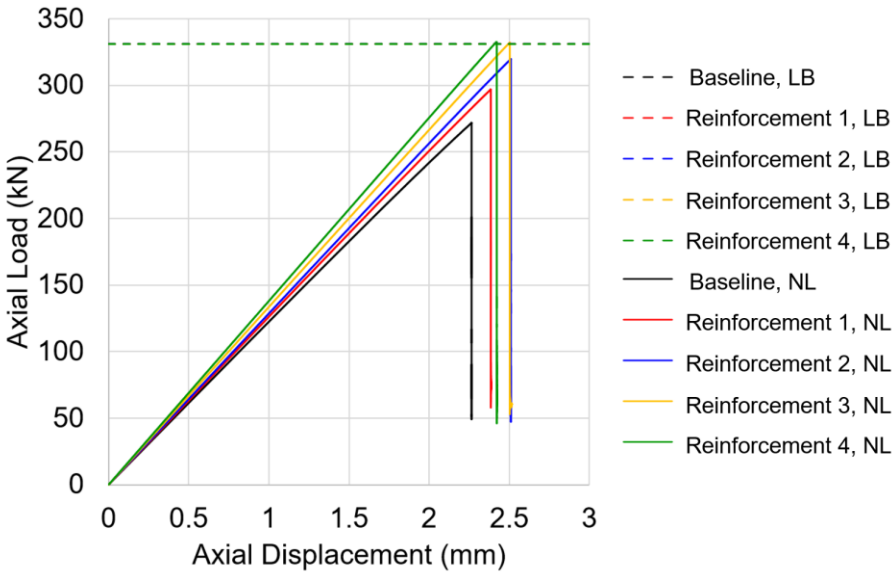

Figure 11. Linear eigenvalue (LB) curve and nonlinear buckling (NL) curves for the composite conical-cylindrical shell with different transition-region reinforcement layups.

The buckling load from the nonlinear analysis of the shell with Reinforcement 3 was 331.9 kN, which is essentially equal to the linear eigenvalue buckling load. The buckling load of the shell with Reinforcement 3 and a radial imperfection amplitude equal to 10% of the wall thickness was 214.0 kN. This results in a normalized buckling load of 0.65, and the reduction in load is solely due to the presence of imperfections. This result is opposite from what was observed for the radius of curvature of 0 mm, which also had a normalized buckling load of 0.65, but where the reduction in load was due to the nonlinear effects. It should be noted that, while the buckling load of the perfect shell may increase by reinforcing the transition region, the reinforced conical-cylindrical shell may be more imperfection sensitive. Therefore, the inclusion of additional plies in the transition did not improve the buckling behavior of the imperfect composite-conical cylindrical shell because it was more sensitive to imperfections, which negated the benefits of adding the reinforcement.

In the end, a KDF is required to account for the difference between the tested buckling load and the buckling load from a linear eigenvalue analysis of idealized geometry. For a conical and cylindrical shell, a significant percentage of the difference between test and analysis is largely attributable to imperfections, which is generally unknown during the design phase. For conical-cylindrical shells it is possible to design the structure so that buckling design load is less sensitive to imperfections, and more sensitive to large displacements and rotations. The large rotations and displacements can be accounted for in the design phase with a geometrically nonlinear analysis. Therefore, it may be possible to use a KDF closer to unity if the buckling load of the shell is more susceptible to the effects of nonlinear geometry, which may result in a more mass efficient design.

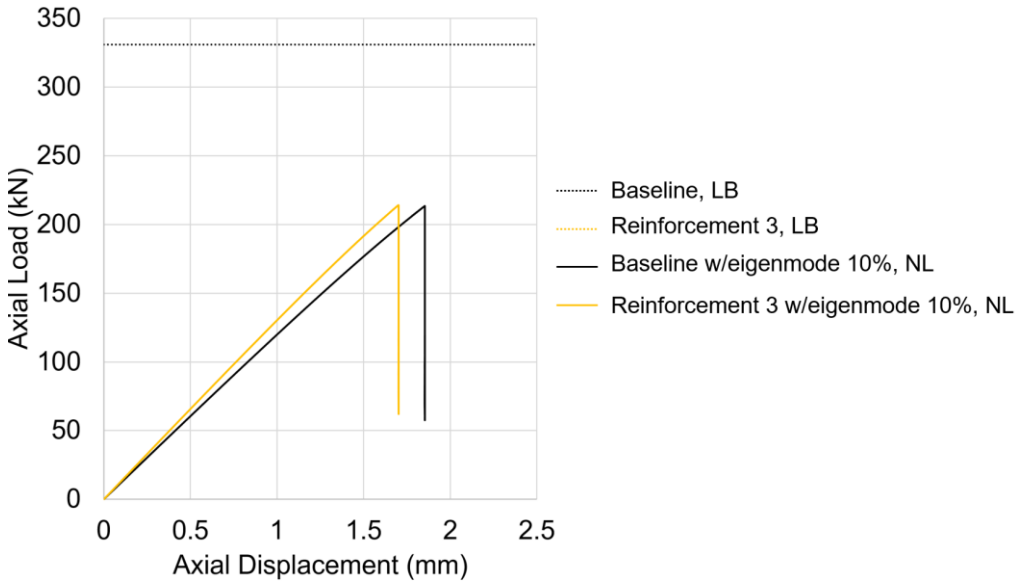

Figure 12. Linear eigenvalue (LB) curve and nonlinear buckling (NL) curves for the composite conical-cylindrical shell with different transition reinforcement layups.

IV. Manufacturing, analysis, and testing of composite conical-cylindrical shells

As discussed above, the results from the numerical analyses were used to identify interesting behaviors of conical-cylindrical shells. These behaviors included, for example, that the effect from geometric nonlinearity could be more significant than radial imperfections. In addition, it was observed that adding reinforcement can seemingly increase the buckling load, but the imperfection sensitivity increases potentially to a point where there could be no added benefit from adding reinforcement. In order to validate these observations, a composite conical-cylindrical shell was manufactured and loaded in axial compression until buckling occurred. After the completion of the first test campaign reinforcement was added the transition region of the original shell and the shell was tested again. The geometry of the test article is presented in Figure 13. The dimensions were slightly different than what was used in the numerical analyses discussed above because the test article had to be scaled down to fit into the test frame.

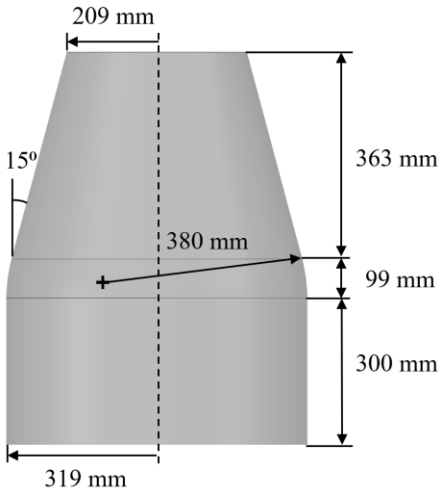

Figure 13. Nominal dimensions of the test article.

The test article was constructed in the Composite Technology Center at NASA Marshall Space Flight Center using the automated fiber placement robot shown in Figure 14. The test article was manufactured using Hexcel's IM7-8552/1 unidirectional tape with a width of 6.35 mm. The nominal material properties are the same as was assumed in the numerical analyses. The layup was an 8-ply quasi-isotropic laminate of $[45/-45/90/0]_S$ and a total laminate

thickness of 1.43mm. The test article was trimmed flat and parallel after manufacturing, and then potted into aluminum end rings to mimic fixed end boundary conditions.

Figure 14. Test article being built on the automated fiber placement robot.

The first buckling test article was designated Composite Conical Cylindrical Shell (3CHELL). The test article was highly instrumented with a combination of 56 unidirectional and biaxial strain gages. It was also painted with a high-contrast black and white speckle pattern for the use of digital image correlation (DIC) to collect full-field data of the strain and displacements. The entire test setup is pictured in Figure 15. Two subcritical load sequences were conducted prior to the final buckling test.

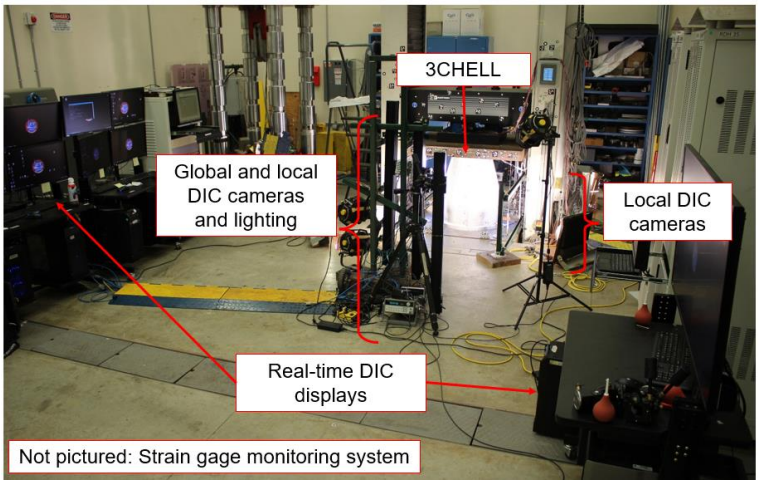

Figure 15. Buckling test setup.

Before the test, a finite element model (FEM) of 3CHELL was created in Abaqus using four-noded reduced integration shell elements (S4R). The FEM included the overlaps of adjacent tows, which were an artifact of the geometry and manufacturing process, and were present because it was specified that there would be no gaps between courses of tows. As seen in Figure 16a, the +45- and -45-degree overlaps can be observed by the orthogrid-like pattern in the conical section. The overlaps were approximated in the FEM with different section properties defined to represent the overlapped areas that have additional +/- 45-degree plies, as shown in Figure 16b by the red, yellow, and dark blue colors. A table of the section properties is presented in Table 5. A Lanczos linear eigenvalue analysis of 3CHELL using this model was completed and resulted in a buckling load of 307.8 kN. In addition, radial imperfections measured by scanning the inner and outer surfaces of the shell using a photogrammetric technique were included into the FEM. A dynamic implicit analysis of 3CHELL with the radial imperfection was also completed prior to the test. For the sake of brevity in this paper, the results from the numerical analyses will be compared by means of

the normalized buckling load calculated using the tested buckling load divided by the linear eigenvalue. The design of 3CHELL is akin to the baseline design from the numerical analyses, except for the features from the tow overlaps. A detailed description of the test set up and analysis is in reference 8.

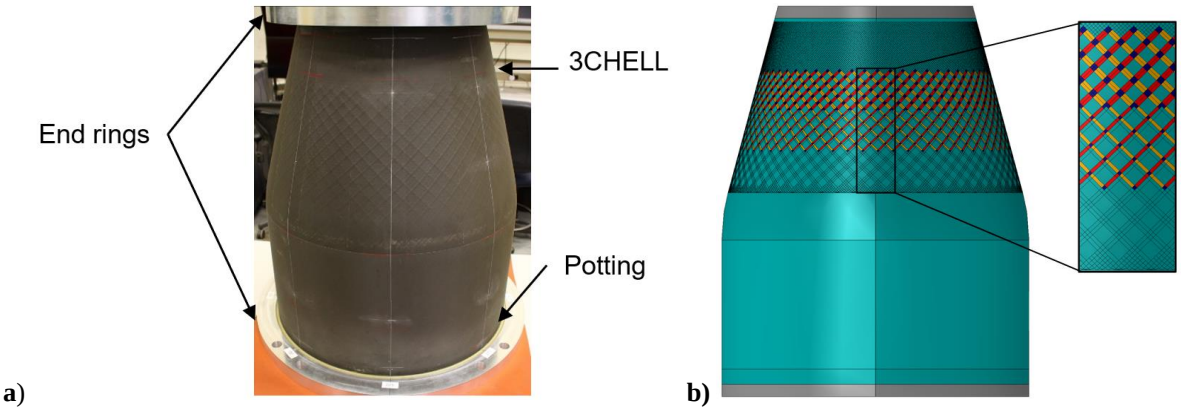

Figure 16. Test article potted in end rings (a) and finite element model of test article (b).

Table 5. FEM Section Properties.

Section	FEM color	Stacking Sequence
Acreage	Cyan	45/-45/90/0/0/90/-45/45
+45 overlap	Red	45/**45**/-45/90/0/0/90/-45/**45**/45
-45 overlap	Yellow	45/-45/**-45**/90/0/0/90/**-45**/-45/45
+45 and -45 overlap	Dark blue	45/**45**/-45/**-45**/90/0/0/90/**-45**/-45/**45**/45
Potted ends	Gray	Al ring/Potting/Acreage/Potting/Al ring

During test, 3CHELL buckled in the cylindrical section at a load of 251.8 kN, Figure 17. This results in a normalized buckling load of 0.82 for 3CHELL. No permanent deformation or material failure was observed, and it was concluded the buckling event was elastic. Therefore, it was decided retest 3CHELL after it was modified by adding reinforcement locally to the transition region to investigate changes in the buckling behavior after modification.

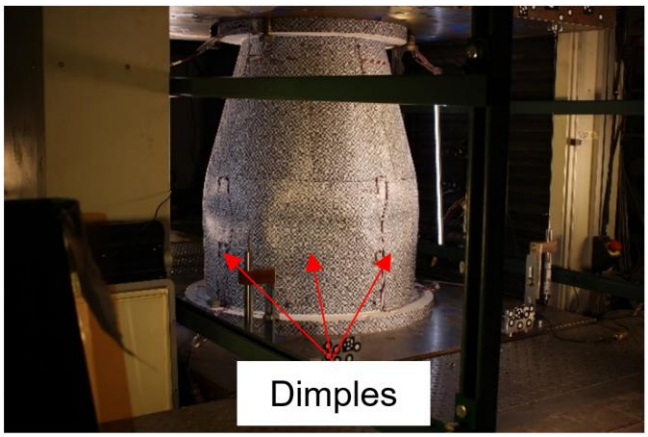

Figure 17. Postbuckled of 3CHELL.

To perform the modification, the test article was removed from the load frame, and the transition region was reinforced with two plies of Toray T1100G 3960 plain-weave fabric that were placed on the inner mold line in the area highlighted in Figure 18a. The top ply encompassed the bottom ply as shown in Figure 18b. Each piece of plain-weave fabric was nominally 0.196 mm in thickness. The plies were bonded using a film adhesive FM209-1, which was approximately 2.54 mm in thickness, and cured using an out-of-autoclave process. The reinforcement plies were

placed on the inside of 3CHELL because the outside was covered with the speckle pattern for DIC. The FEM of 3CHELL was modified to account for the additional reinforcement. The fabric was assumed to have a modulus of elasticity of 77.9 MPa in the fiber direction, a modulus of elasticity transverse to the fiber direction of 86.9 MPa, a shear modulus equal to 5.1 MPa, and a Poisson's ratio of 0.05 [14]. The stiffness of the reinforcement plies added to the transition had approximately the same stiffness as the Reinforcement 3 configuration in the numerical analyses discussed above. The reinforced version of 3CHELL was referred to as Re3CHELL.

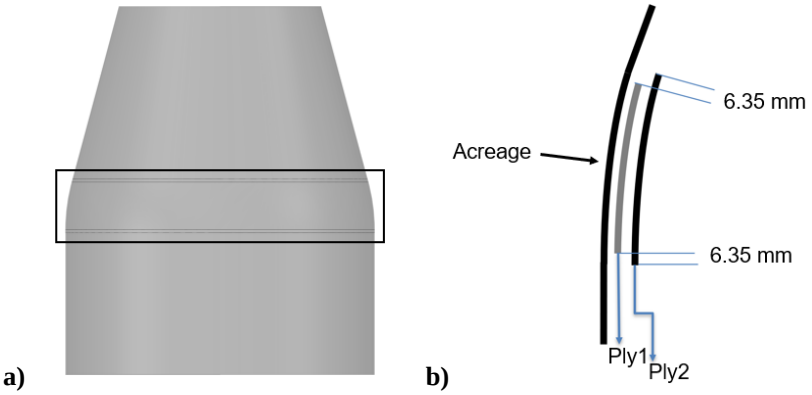

Figure 18. Reinforcement area (a) and reinforcement detail (b)

A dynamic-implicit geometrically nonlinear analysis with measured radial imperfections was completed prior to test of Re3CHELL. For the sake of brevity in this paper, the results from the numerical analyses will be compared by means of the normalized buckling load calculated using the tested buckling load divided by the linear eigenvalue buckling load. The test article, Re3CHELL, was instrumented, and the test was conducted in the same manner as 3CHELL. Buckling occurred in the conical section of Re3CHELL at a load of 268.7 kN, Figure 19. The linear eigenvalue for Re3CHELL was 314.0 kN. The tested buckling load divided by the linear eigenvalue equals a normalized buckling load of 0.85.

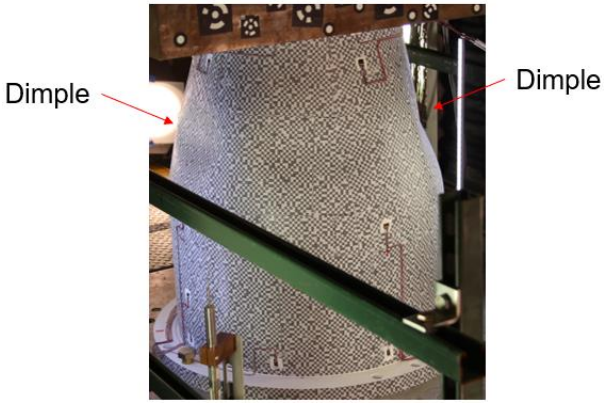

Figure 19. Postbuckling of Re3CHELL.

The 3CHELL design was similar to the baseline numerical model and the Re3CHELL analysis was similar to the Reinforcement 3 numerical model. As previously discussed, the predicted normalized buckling load was 0.65 for both the baseline shell with geometric imperfections and the shell with Reinforcement 3 and geometric imperfections, Figure 12. The addition of reinforcement made the conical-cylindrical shell more sensitive to imperfections and the normalized buckling load did not change. A similar observation can be made with the test of 3CHELL and Re3CHELL. That is, the normalized buckling load for both test articles were similar, 0.82 and 0.85 respectively. This confirms that adding additional reinforcement may not increase the buckling load as intended because of increased sensitivity to radial imperfections of the reinforced shell.

V. Conclusions and design recommendations

Due to advances in manufacturing and numerical methods, it is possible to combine conical and cylindrical shell components, and potentially save mass by eliminating the heavy interface ring that separates the two structures. The results of this paper showed that current buckling knockdown factor recommendations in NASA SP-8007 and NASA SP-8019 may not be suitable for conical-cylindrical shells because those recommendations may not be conservative in some cases. In addition, though an increase in the linear eigenvalue may be achieved by either increasing the radius of curvature of the cylinder-cone transition region or adding reinforcement to this transition region, the imperfection sensitivity was shown to also increase, which can offset some or all of the increase in buckling load when geometric nonlinearities and imperfections are considered. If an imperfection sensitivity study is performed with the intent of developing a design specific knockdown factor, it is recommended to consider imperfection shapes other than the first linear eigenmode. It was observed that the eigenmode imperfection did not significantly influence the buckling response with an imperfection amplitude of 10% of the shell wall thickness. Finally, because imperfections are largely unknown during the design process, it may be more beneficial to rely on the predictable behavior of the large rotations and displacements at the transition. In this case, it may be possible to benefit from a higher knockdown factor by designing a conical-cylindrical shell more susceptible to the nonlinear behavior which can be captured numerically during the design process since this design would be less sensitive to radial imperfections.

Acknowledgements

The authors would like to acknowledge Dr. Nathaniel Gardner and Dr. Cyrus Kosztowny, both from NASA Langley Research Center, and the Marshall Space Flight Center Structural Test Branch (ET30) for their significant contributions to the 3CHELL and Re3CHELL test. In addition, this work would have not been completed without the funding from Marshall Space Flight Center's Technical Excellence fund.

References

[1] Rotter J. M., "The Buckling and Plastic Collapse of Ring Stiffeners at Cone/Cylinder Junctions." *Proceedings Int. Colloquium on Stability of Plate and Shell Structures*, Ghent, Belgium, 1987, pp. 449-456.

[2] Teng J.G., "Cone-Cylinder Intersection Under Internal Pressure: Axisymmetric Failure," *Journal of Engineering Mechanics*, Vol. 120, No. 9, 1994, pp. 1896–1912.

[3] Teng J.G., "Cone-Cylinder Intersection Under Internal Pressure: Nonsymmetric Buckling," *Journal of Engineering Mechanics*, Vol. 121, No. 12, 1995, pp. 1298–1305.

[4] Flores F.G., Godoy L.A., "Postbuckling of Elastic Cone-Cylinder and Sphere-Cylinder Complex Shells," *International Journal of Pressure Vessels and Piping*, Vol. 45, No. 2, 1991, pp. 237–258.

[5] Anwen, W., "Stresses and Stability for the Cone-Cylinder Shells with Toroidal Transition," *International Journal of Pressure Vessels and Piping*, Vol. 75, No. 1, 1998, pp. 49–56.

[6] Patel B. P., Nath, Y., Shukla, K.K., "Nonlinear Thermo-Elastic Buckling Characteristics of Cross-Ply Laminated Joined Conical- Cylindrical Shells," *International Journal of Solids and Structures*, Vol. 43, No. 16, 2006, pp. 4810–4829.

[7] Singh S., Patel B.P., and Nath Y., "Postbuckling Behavior of Angle-Ply Laminated Joined Circular Conical-Cylindrical Shells," *AIAA Journal*, Vol. 45, No. 4, 2007, pp. 942–949.

[8] Rudd M.T., Schultz M.R., Gardner N.W., Kosztowny C.J.R., Bisagni C., "Testing of a Composite Conical-Cylindrical Shell,", AIAA 2023-1525, AIAA SciTech Forum, January 2023.

[9] Hilburger M.W., "Buckling of Cylindrical Shells." NASA Space Vehicle Design Criteria (Structures), NASA SP-8007 rev 3, 2020.

[10] Weingarten V.I., Seide P., "Buckling of Thin-Walled Truncated Cones," NASA Space Vehicle Design Criteria (Structures), NASA SP-8019, 1968.

[11] Schultz, M.R., Sleight, D.W., Gardner, N.W., Rudd, M.T., Hilburger, M.W., Palm, T., Oldfield, N.J., "Test and Analysis of a Buckling-Critical Large-Scale Sandwich Composite Cylinder," AIAA 2018-1693, AIAA SciTech Forum, January 2018.

[12] Abaqus/Standard User's Manual. Version 2021 ABAQUS. Inc. USA; 2021.

[13] Clarkson, E., "Hexcel 8552 IM7 Unidirectional Prepreg 190 gsm & 35%RC Qualification Statistical Analysis Report," Technical Report NCP-RP-2009-028 Rev B; 2019.

[14] Toray 3960 Prepreg System Data Sheet, https://www.toraycma.com/wp-content/uploads/3960-Prepreg-System.pdf , last accessed October 2023.